Multipass lock-in thermography for the study of optical coating absorption

Camille Petite, Rémi Marcouillé, Antonin Moreau, Hélène Krol, Catherine Grèzes-Besset, Julien Lumeau, Laurent Gallais

Multipass lock-in thermography for the study of optical coating absorption

Camille Petite,[1,2] Remi Marcouille,[2] Antonin Moreau,[2] Helene Krol,[1] Catherine Grezes-Besset,[1] Julien Lumeau,[2] Laurent Gallais[2*]

[1]*CILAS Etablissement de Marseille, 600 avenue de la Roche Fourcade, Pole ALPHA Sud - Saint Mitre, 13400 Aubagne – France*
[2]*Aix Marseille Univ, CNRS, Centrale Marseille, Institut Fresnel, UMR 7249, 13013 Marseille, France*
**Corresponding author: laurent.gallais@fresenel.fr*

Received 6 Oct 2021; revised 21 Dec 2021; accepted 23 Dec 2021; posted 4 Jan 2022; published 28 Jan 2022 https://doi.org/10.1364/AO.445045

The development of high-power lasers requires optics with very low absorption to avoid detrimental thermal effects. In this work, we discuss our recent developments on the lock-in thermography to measure absorption. We applied this technique in a multipass configuration to increase the effective power on the tested samples. We present a system based on a kW-class ytterbium fiber laser operating at 1.07 µm wavelength, which enables exposing samples to 5 kW effective power and measuring absorption in the ppm range. The implementation, calibration procedure, and obtained performances are discussed with some applications to single-layer coatings of HfO_2, Ta_2O_5, TiO_2, Nb_2O_5, and SiO_2 deposited by plasma-assisted electron beam deposition.

1. INTRODUCTION

Since Theodore Maiman demonstrated the first laser in the 1960s [1], research in this field has led to new concepts and systems to increase the laser peak power and energy [2–6]. Petawatt-class lasers are now available, and the exawatt range is the future goal for mode-locked lasers [7], as well as megajoule laser systems with nanosecond pulses [8,9]. An increase in continuous wave (CW) laser power is also driven by industrial needs for machining and defense applications [10–12]. The most powerful commercial CW lasers now reach more than 100 kW [13].

Such high power implies the specific needs of optics with very low absorption to avoid detrimental thermal effects, including the damage of optical components [14]. Optical interference coatings are essential components of laser systems. They are obtained through physical vapor deposition technologies, and their absorption levels are strongly dependent on the material and deposition parameters.

Consequently, various measurement methods have been developed to evaluate absorption below the parts per million (ppm) level. They are all based on the photothermal effects obtained with a pump laser [15,16]. A strong advantage of this method is that absorption can be dissociated from scattering, as opposed to other photometric techniques based on measurements of losses, such as cavity ring down [15,17]. Laser calorimetry (LC) [18,19] is based on the direct measurement of the temperature rise of a sample with a thermocouple or a transductor. Then, the thermal signal is related to the absorption by an appropriate calibration. This is a reference method in the field [12]. Another way to determine the absorption is to detect effects related to the temperature rise. Photothermal deflection (PDT) [21–24] or surface thermal lensing (STL) [25] use the modification of the surface and of the refractive index (i.e., the optical path) that is probed by a laser beam and linked to the absorption through a calibration procedure. Interferometric techniques can also be used to measure temperature-induced modifications. Common-path interferometry (CPI) [26,27] uses the refractive index change caused by the absorbed energy of a pump beam to produce self-interference of a probe beam that is detected by a photodiode. Self-phase modulation (SPM) [28,29] uses the variation of the transmission spectra shape of a Fabry–Perot interferometer caused by a variation of optical path due to the introduction of a pumped sample in the cavity to obtain the absorption. Finally, we can also cite photoacoustic spectroscopy (PAS) [30–32] as another measurement technique using a pulsed laser as a pump and the detection of acoustic waves generated by the local thermal variation inside the sample. With thermography, the temperature can also be measured using a thermal camera [33]. In this case, the measurement method is referred to as photothermal radiometry (PTR) [34]. This method will be investigated further in this study.

In this work, we studied the lock-in thermography (LIT) technique [35]. The temperature rise on a sample leads to infrared radiation according to Planck's law. We have to keep in mind the real radiation of a sample also depends on a

material and wavelength-dependent parameter: emissivity. By detecting such radiation, thermal cameras provide a signal map linked with a proper calibration to the temperature distribution on the sample. For very low absorption, the thermal signal can be hidden by noise or other bias on the image as a narcissus effect (i.e., the thermal image of the sensor reflected on the observed sample) or reflected radiation from the surroundings. The LIT technique can be used to avoid such issues [36]. To perform lock-in measurements, a laser modulated in amplitude at a known frequency is used to generate a thermal signal with the same frequency. In the simplest case of a sine signal without any noise, the Fourier transform only shows a peak at the modulation frequency with ½ of the signal amplitude and another at 0 Hz, the mean signal value. For a noisy signal, the Fourier transform shows peaks over a wider range of frequencies. By selecting only the signal at the modulation frequency, it is possible to provide a de-noised thermal image of the sample. The interesting aspect of this technique is that one can directly obtain absorption mappings with a single measurement, whereas the classical photothermal methods requires scans on optics.

In the following, we present the LIT principles and an experimental demonstration with the objective of finding the conditions to maximize the signal-to-noise ratio. Then, we present a metrological study of our setup to obtain a calibrated measurement with a known level of confidence. Finally, we use this system to perform absorption measurements of various single-layer coatings and to study the effects of layer fabrication parameters on absorption.

2. DEVELOPMENT OF LIT EXPERIMENT

A. Use of lock-in technique to enhance the signal to noise ratio of active thermography

To understand the benefit of the LIT technique, we first estimated the typical temperature reached in a sample submitted to laser irradiation. A model relying on the assumption of a Gaussian laser beam absorbed by a semi-infinite medium was presented in various references [37–39]. The steady state temperature rise at the center of beam ΔT is given by

$$\Delta T = \frac{AP}{2Kw}\sqrt{\frac{2}{\pi}} \qquad (1)$$

where A is the optical absorption by the medium (defined as the proportion of the input power coupled in the medium) of the laser beam of power P, w is the beam waist at $1/e^2$, and K is the thermal conductivity of the medium. Equation (1) is, however, based on the hypothesis of a semi-infinite substrate that can be considered when the spot size is much lower than the sample thickness. In order to obtain a better description of the temperature rise, we also conducted numerical simulations using a finite element model (FEM) simulation software (COMSOL Multiphysics). Based on the FEM, the heat equation is solved taking into account the Gaussian surface heat source related to absorption, the finite size of the sample and radiation losses at the boundaries. The results are compared in Fig. 1 for a fused silica substrate with a thickness of 2 mm and 25 mm diameter. The thermal parameters of the silica we used are K = 1.38 W.m^{-1}.K^{-1} for thermal conductivity, Cp = 770 J.Kg^{-1}.K^{-1} for heat capacity and ρ = 2200 Kg.m^{-3} for density [40]. All simulations are performed with 1 ppm of absorption and a laser power varying between 2.5×10^{-1} to 2×10^{3} W.

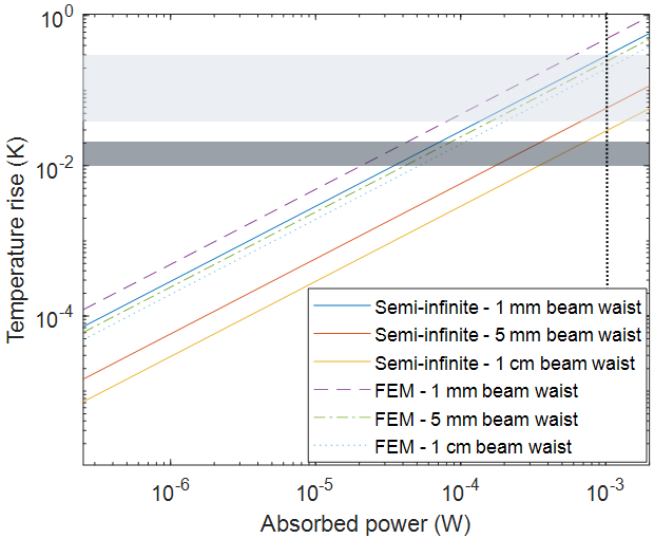

Fig. 1. Temperature elevation for 2 mm thick fused silica substrate (K = 1.38 W.m^{-1}.K^{-1}) illuminated by a Gaussian laser beam as a function of absorbed power and for various laser beam waists at 1/e^2. The light grey band is the noise equivalent temperature difference (NETD) of a standard bolometric sensor and the dark grey band is the NETD for high-performance thermal cameras [35]. The black dotted line emphases the case of 1 ppm of absorption and a kilowatt laser, an absorbed power of 10^{-3} W leads to a temperature rise of 10^{-2} °C.

For small spots (1 mm), the two models yield similar results, but for larger spots (10 mm), the analytical model is no longer valid. To identify the validity limit of the semi-infinite model, we plot in Fig. 2 the comparison of the two models for different beam waists but for the same silica. This analysis evidences a divergence between the models for beam waists larger than 3×10^{-3} m.

Therefore, our discussion will be based on FEM simulations.

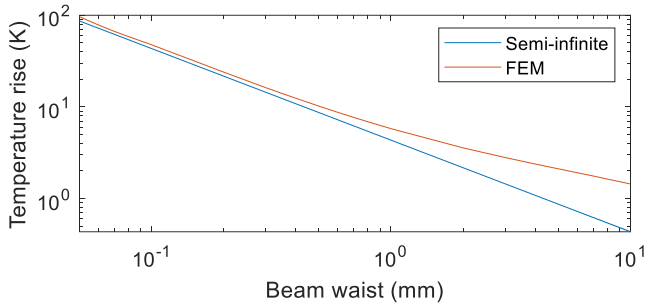

Fig. 2 : Evolution of the temperature rise for both semi-infinite and FEM models as a function of the Gaussian laser beam waist (radius at $1/e^2$).

The noise equivalent temperature difference (NETD) provides the minimal temperature measurable by a thermographic device. The NETD is defined as the difference in temperature on the scene that gives a signal equals to the noise. This noise is determined by calculating the mean value for all pixels of the standard deviation of the temporal signal. For a standard bolometric sensor, the NETD is approximately 40–300 mK depending of the camera [35], but it can drop to 10 or 20 mK for high-performance cameras based on cooled infrared detectors. As a consequence, we can see in Fig. 1 that the absorbed power is detectable for both types of thermal cameras. For typical high-performance optics with 1 ppm absorption, a 100-W laser is needed to achieve the detection of a temperature change, and a kilowatt-class laser is required to achieve adequate sensitivity on a cross-section area of the laser of 1 cm^2.

Another way to improve the sensitivity of thermography is to use a lock-in technique to extract the signal from the noise. Unlike passive thermography, LIT uses a modulated laser beam to obtain a modulated thermal response at the same frequency. This technique allows the separation of temperature variation in the sample from other non-modulated thermal or noise contributions. Consequently, all the other signal frequencies are removed. By measuring the noise on an LIT image and the mean of 2048 images used in the lock-in technique, a dramatic increase of signal to noise ratio of 18 times was observed for a 16-period LIT measurement. Note that the frequency of 0 Hz, representing the mean signal, is also canceled. Thus, LIT has a very low sensitivity to environmental bias. The principle of LIT is illustrated in Fig. 3.

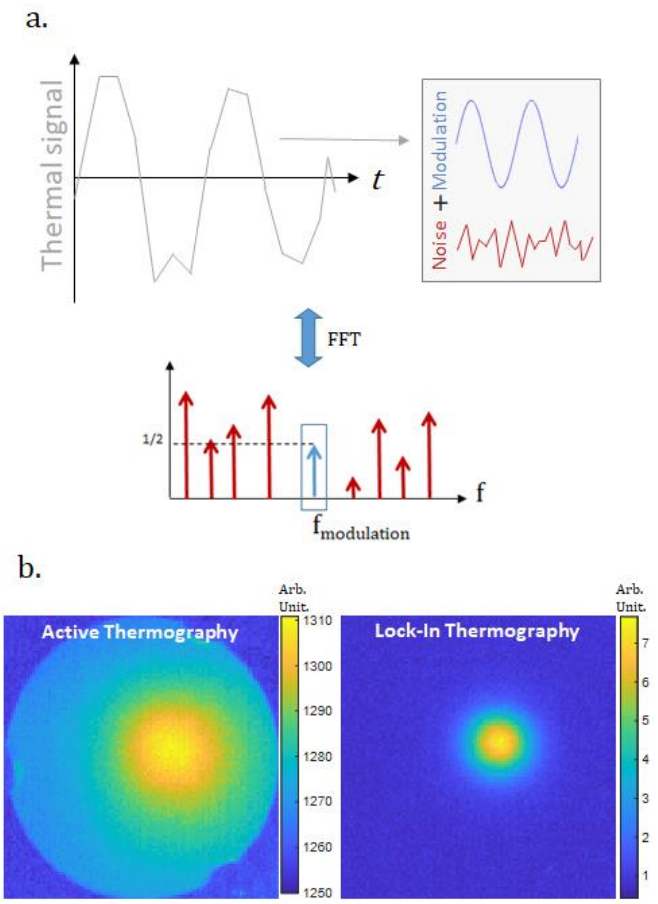

Fig. 3. On part a. the principle of LIT. Thermal images are taken with an infrared camera while the laser is modulated (sine wave). The camera signal is composed of the modulated signal (blue curve) and the noise (red curve). A fast Fourier transform is used to separate modulated signal from the noise by filtering at the modulation frequency. On b. part, an image taken with active thermography on the right and a LIT image taken on the same sample on the left.

B. Use of a multipass configuration to increase the thermal signal

All photothermal methods for absorption measurements are based on measurements of physical effects related to a very small temperature rise. Indeed, as these methods are used to measure very low absorption, only a few ppm of the laser power is useful for generating the thermal effect. The conceptual basis of the setup we developed was to recycle the laser beam and overlap it on the same spot on the measured sample. After the first pass through the sample, the reflected and transmitted beams are redirected toward the sample with highly reflective mirrors. This approach is then repeated several times with the new transmitted and reflected beams until the desired total power on the measured sample is achieved. The laser beam is collimated in order to neglect the divergence of the beam and keep a constant beam radius over a few meters. To avoid the multiplication of mirrors on each

pass, we aligned the setup to ensure that the output reflected and transmitted beams at each pass are precisely overlapped.

This principle was implemented three times using the LIT setup (Fig. 4). The number of passes is limited to maintain a compact setup and minimize all incidence angles. In our case we stay under 20° angle, because the optical function (reflection and transmission) depends on the angle. So we try to stay on a minimized angle range. So the measured absorption is an average value of the absorption at all incident angles. However, in case of single layers (as studied in this paper), this change of absorption with the angle of incidence can be neglected. The number of passes can be increased if a higher power is required. The beam was sent through a sample with a beforehand unknown transmission and reflection (i.e. it could be a mirror, a beam splitter or an anti-reflective coating). The transmitted beam is reflected on so-called "collecting mirrors" CM1, while the reflected beam is reflected by another mirror CM'1. The reflected beams are then redirected toward the sample with two "deflection mirrors," DM1 and DM'1. This principle is used again with the new overlapped beams that are reflected and transmitted by the sample to illuminate the sample a third time with the use of mirrors CM2, CM'2, DM2, and DM'2. The multipass setup has also the advantage to allow to increase the laser irradiance on the sample while keeping a low irradiance on the other optics.

A CW nonpolarized single transverse-mode laser (SPI redPOWER® QUBE) with a power ranging from 150 W to 1.5 kW at a wavelength of 1070 nm was used as a source. The modulation was obtained by applying a 0–10 V signal on a dedicated external input of the laser and generated with a National Instruments NI USB-6211 card. Software was written by the authors to control the NI card. The Gaussian beam was guided to the setup with a single-mode fiber and collimated to 3.34 mm waist at $1/e^2$. To ease the alignment of the setup, a visible collimated laser diode at 633 nm was introduced in the beam path. The collinearity of both the power laser beam and alignment beams was achieved with two 50 mm diameter infrared mirrors (UVFS Laser Line Mirror, Eksma). All the collector and deflection mirrors were 25 mm diameter broadband mirrors (BB-E03, Thorlabs). The camera was an Optris PI230 operating in the range of 8–14 µm. The 35 mm focal – f/1.6 aperture of the camera optics yielded an NETD of 300 mK and a spatial resolution of approximately 200 µm per pixel on the sample. The sample was mounted on a Thorlabs KS1SC - Kinematic Self-Centering Mount and on a two-axis Newport UTS50PP motorized linear stage.

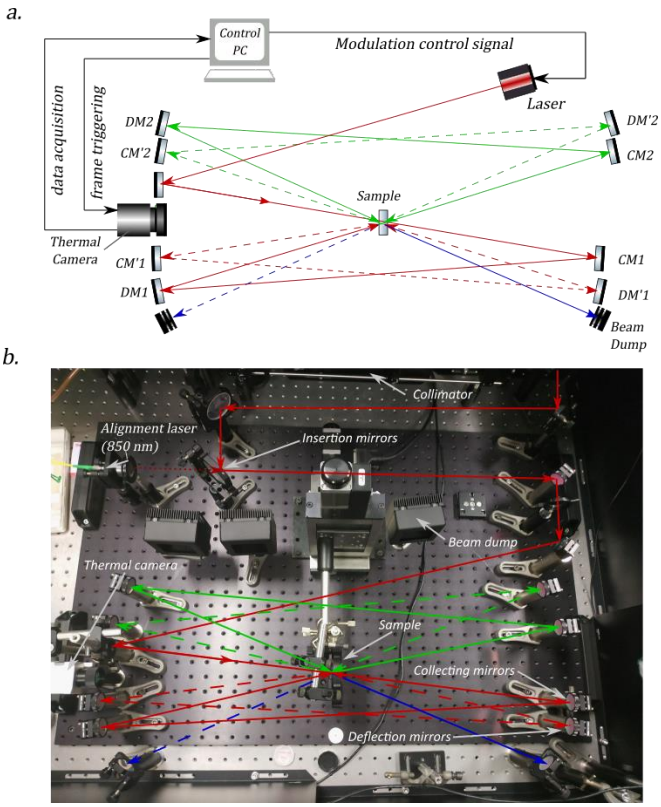

Fig. 4. Schematic (a.) a photography (b.) of the multipass LIT setup. The beam color is changed after each pass for clarity. Here, the sample acts as a beam splitter, to consider every case of reflection and transmission rates of samples .

C. Effect of acquisition time on LIT setup performance

The LIT measurement was performed by acquiring an image of the sample emission with a known frequency. Then, the photothermal signal was obtained by applying a fast Fourier transform to each pixel of each image using the *fft* and *fftshift* Matlab core functions. We applied a bandpass filter centered on the fundamental and the harmonics of the modulation frequency with a bandwidth of 3 mHz. To filter our signal, we select the needed frequency in the discrete Fourier transform. This means the equivalent filter has a bandwidth at each selected frequency $\Delta f = f_s/N$ with f_s the sampling frequency (6.4 samples per second in this study) and N the number of samples (2048 points in this study). This implies a bandwidth of 3 mHz in this work. For sine modulation, as the thermal response was also a sine wave, we selected a band-pass filter at the modulation frequency

However, lasers often have a minimum power threshold (that value for the laser used in this paper is 150 W). Consequently, the sine wave could only be applied between 150 W and 150+ΔP W with ΔP the change in power. Because the LIT technique extracts the thermal effect due to the ΔP variation, this modulation technique is not the most efficient

in this case. An alternative solution was to apply a square waveform (i.e., by switching the laser on and off) in order to increase the modulation amplitude, but the thermal response in this case contained harmonics, as shown in Fig. 5.

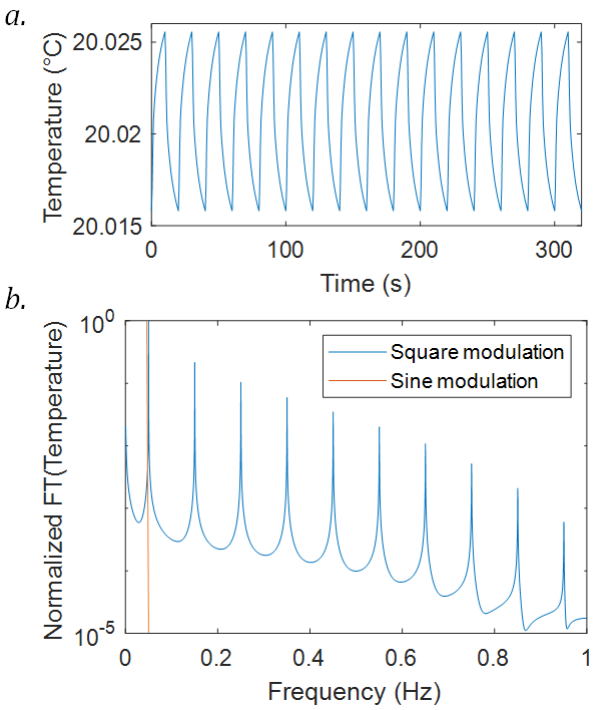

Fig. 5. On a. the simulated steady state thermal response of a fused silica substrate illuminated with a square signal at 0.05 Hz and with 1 ppm of surface absorption. On b., the frequency spectrum of this thermal response. The amplitude is normalized by the amplitude of the fundamental and the null frequency is cutted from the data because we focus on the frequencies of the modulated part of the thermal response.

The spectrum shows a fundamental at the modulation frequency and harmonics at odd multiples of the fundamental frequency. To maximize the signal level, we used the fact that all harmonics contribute to the total photothermal signal and define it as the sum of the amplitudes of the fundamental and harmonics. By applying this procedure to each pixel of the image, we obtain an LIT image corresponding to the temperature variation profile in arbitrary units. According to the spatial profile of the laser, the photo-thermo-induced image also shows a Gaussian profile. To account for the non-uniform distribution, we fitted the measured signal with a 2D Gaussian function using the MATLAB fitting toolbox, and extracted an average amplitude representative of the measurement. Defects are excluded from this fit to obtain the baseline absorbing level of the coating. However, when these defects are too close to the center of the Gaussian, too numerous or too absorbent, it can lead to an overestimation of the LIT signal. This is due to the thermal diffusion of the defects, as well as the processing of these defect areas in the image. Note that LIT signal is linked to temperature and absorption but a dedicated calibration is needed to get the conversion to a physical unit. This is the purpose of the part 3.A.

To choose a proper modulation frequency, we first simulated the effect of the frequency on the temperature for a fused silica substrate, with a surface absorption of 1000 ppm and a sine illumination of amplitude 150 W. We also measured the LIT signal of a Nb_2O_5 single layer deposited on a Corning 7980 substrate with 1000 ppm absorption. As presented in Fig. 6, the simulated temperature change and measured LIT signal decay as the inverse square root of the modulation frequency [35]. In order to maximize the signal amplitude, we choose a low modulation frequency of 0.05 Hz.

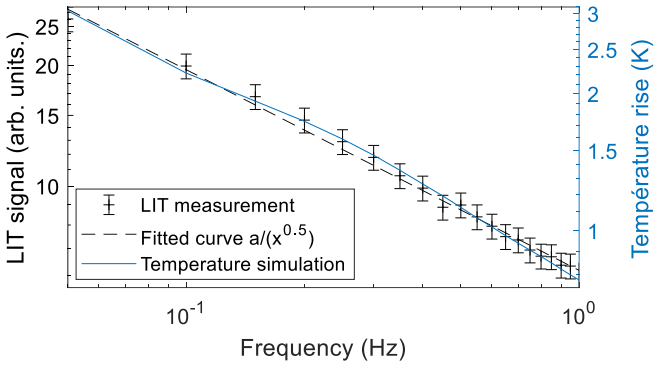

Fig. 6. Temperature variation and LIT signal dependence with frequency. LIT signal is measured on a Nb_2O_5 thin film deposited on a Corning 7980 substrate exposed with 150 W laser power at 1.07 µm. The temperature is simulated with FEM within the same conditions except for the waveform that is taken as a sine function. The error bars are chosen for a relative uncertainty of repeatability of 1.7 % and lead to a 2.4 % total uncertainty on LIT signal (uncertainty calculus are presented on part 3). These error bars are presented with a confidence factor of 3 (99.7 % of measurements).

Heretofore, we have discussed signal evolution with experimental parameters. However, as mentioned above, the main interest of the lock-in technique, it to increase the signal to noise ratio, and thus the noise must be analyzed, especially with respect to the measurement duration and modulation frequency. The noise is defined, as the mean value for all pixels of the standard deviation of the temporal signal. To ease the noise measurement, we assume the noise variations are negligible. As a consequence, the measurement of noise can be performed on a non-illuminated zone of the thermal image (20 × 20 pixels in our case). The relative standard-deviation σ_{Rnoise} of the noise measurement only depends on the number of measurement points N by using the formula:

$$\sigma_{Rnoise}{}^2 = \frac{1}{2(N-1)} \qquad (2)$$

In Fig. 7, the measured noise evolution is plotted as a function of the acquisition time and modulation frequency. A decrease in noise is observed on both plots and can be modeled as follows [35]:

$$\langle A_{noise} \rangle = \frac{2}{\sqrt{f_{mod} . t_{acq}}} NETD \quad (3)$$

where A_{noise} is the average temperature noise amplitude and t_{acq} is the acquisition time.

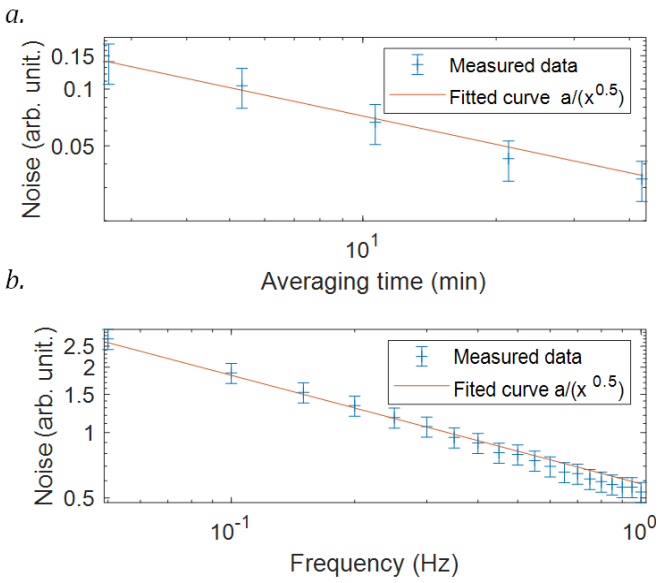

Fig. 7. Dependence of noise on the measurement time on part a. and with modulation frequency on part b. Each measurement is taken with the same number of points and the error bars are presented with a confidence factor of 3 (99.7 % of measurements).

3 MEASUREMENT METHODOLOGY AND ASSOCIATED UNCERTAINTIES.

A. Calibration procedure of the LIT setup

The absorption value is not directly obtained from the LIT measurements, and the software development kit of the camera does not provides a temperature but a signal in arbitrary unit; so a calibration procedure is required. Different strategies can be used for this purpose. The first is to perform a thermal calibration of the setup to relate the signal to the temperature rise of the sample and then to relate the temperature to a theoretical model to estimate the absorption [20]. The second method involves heating the sample with a heater. Assuming that heater, that provides a heating power, and sample are in thermal equilibrium, the measured signal in these conditions will be the same as the one measured with an equivalent absorbed power in the sample. Given the laser power, the absorption can be determined [15,22,41]. The calibration curve (i.e., the signal function of absorption) can also be determined using a set of known standards with different absorptions [36,42]. The procedure involves determining the absorption on one reference sample measurable using a commercial spectrophotometer. Then, the behavior of the reference sample under calibration conditions is extrapolated for all ranges of absorptions [27,43], assuming the linearity of the measured signal with respect to the absorption.

Here, we used the approach based on reference sample with a high absorption and measured the LIT signal as a function of absorbed power to obtain a calibration curve of the measured signal on the absorbed power. Then, given the laser power and the extrapolation of the calibration curve, we can determine the absorption of any sample with the same thermal properties. Our reference sample was prepared by deposition of a Nb_2O_5 single layer with a Bühler SYRUSpro 710 plasma-assisted electron beam deposition (PIAD) machine. We used a reduced flow of O_2 during the deposition process to obtain a nonstoichiometric layer and increase the absorption. Losses were measured with a commercial spectrophotometer (Lambda 1050, PerkinElmer), and the losses (a few percent) were assumed to be mainly related to absorption (i.e. the scattering is assumed to be negligible). The LIT signal was measured at different powers for the reference sample. To avoid high temperature and potential damage or irreversible effects (annealing), the mean laser power was maintained between 1 and 10 W by modulating it with the internal modulation of the laser at kilohertz frequency with 60 µs and 150 W pulses per period. This corresponds to a high frequency modulation at kHz within the low modulation (0.05Hz) of our LIT system. The mean power was controlled by the pulse frequency. The mean power was controlled by the pulse frequency. An example of a calibration curve is shown in Fig. 8.

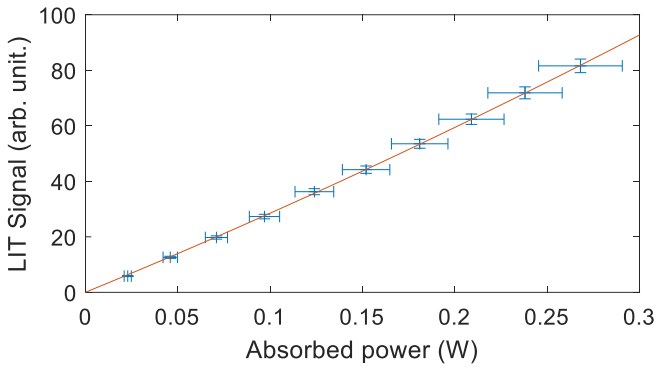

Fig. 8. Calibration curve measured on a reference sample with 2.4% absorption losses. The curve was fitted with a second order model $s = pP_{abs}^2 + nP_{abs}$ with p = 121 a.u./W² and n = 273 a.u./W. Error bars are presented with a confidence factor of 3 (99.7 % of measurements).

The dependence of the absorption power on the LIT signal shows a second-order polynomial behavior, owing to the nonlinear temperature sensitivity of the camera. But to deduce absorption from the curves we fitted the data with the following equation:

$$P_{abs} = AP = as^2 + bs \quad (4)$$

where P_{abs} is the absorbed power, s is the LIT signal, and $a = -6.6\times10^{-6}$ W/a.u.²-and $b = 3.9\times10^{-3}$ W/a.u. are the fitted parameters. With such a calibration, the absorption A of any sample can be calculated with the measurement of the laser power P.

The thermal signal and the LIT signal depends on the emissivity of the samples. Therefore, we should multiply our thermal signal by the emissivity of samples. But in this work all thermal acquisitions were made without any emissivity correction because we assumed that all samples and reference samples had the same emissivity. To verify this assumption, we measured the effective emissivity, as shown by Stewart et al. [33]. This measurement was performed by placing the samples on a temperature-controlled surface. The emissivity in the camera software was then adjusted so that the sample temperature matched the set temperature (100°C). The different samples investigated in this work were tested: uncoated fused silica substrates and single layers made of Nb_2O_5 and HfO_2 with different thicknesses and stoichiometries and deposited on fused silica substrates. No significant differences in emissivity were observed for these samples. This means, emissivity correction is not necessary in this work where only single layers are studied. However, we should point out that in the case of multilayer coated substrates and substrates of different materials (fused silica / borosilicate), significant differences are observed (typically 0.02 to 0.1, depending on the component), and emissivity corrections would be required because the initial assumption is no longer valid in this case.

B. LIT measurements uncertainty

The uncertainties in the LIT absorption measurements were investigated thoroughly. They have three main origins: LIT signal uncertainty, laser power uncertainty, and calibration uncertainty.

The uncertainty of the signal is associated with several sources, related to measurement and processing.

Regarding LIT signal measurement uncertainty, we evaluated the reproducibility of this signal by repeating the measurement procedure. A relative standard deviation of 7.8% at a signal of approximately 0.8 arb. units is measured. However, this value drops to 1.7% at approximately 5.5 arb. units. It is important to bear in mind that the minimum signal where the repeatability was measured is 0.8 arb. unit. (corresponding to 20 ppm of absorption with 150 W). This uncertainty probably increases with a lower signal.

Signal uncertainty can also arise from lock-in processing: by using the FEM, we can calculate the variation of the LIT signal during the transient and stationary heating of the sample. A thermal simulation of 4000 s is used to calculate this signal with a sliding window of 320 s (16 periods) as shown in Fig. 9. The variation of the signal leads to an error that decreases with time. It drops from 5.6% for a measurement starting at the same time as the laser modulation to 0.3% when the sample reaches thermal equilibrium. Another contributor to the signal uncertainty is linked to the number of applied periods to perform lock-in detection. When this number of applied periods increases on a steady state signal, the signal decreases and tends toward a value we assume to be the unbiased value we choose as a reference. This value is used to calculate the relative error for different numbers of lock-in periods. Fig. 10 shows an error below 1% in every case and mainly independent of the absorption level. If we assume a uniform distribution of the measurement value in our error, we can take a standard deviation $\sigma = \frac{Error}{2\sqrt{3}}$ [44]. In the worst case, this leads to a relative uncertainty of 1.6% for the measurement taken in the transient regime of temperature and 0.3% in the case of a four-period measurement. The total lock-in uncertainty is 1.6%.

The last processing source of the error is related to the Gaussian fitting of the LIT image. The MATLAB fitting toolbox used for the Gaussian fit provides an uncertainty for this fit of approximately 0.3% for a sample with a signal measurement of 0.1 arb units, which decreases to 0.01% for a signal of 142 arb. units.

If we consider the worst case, the relative uncertainty of the signal is 8 %.

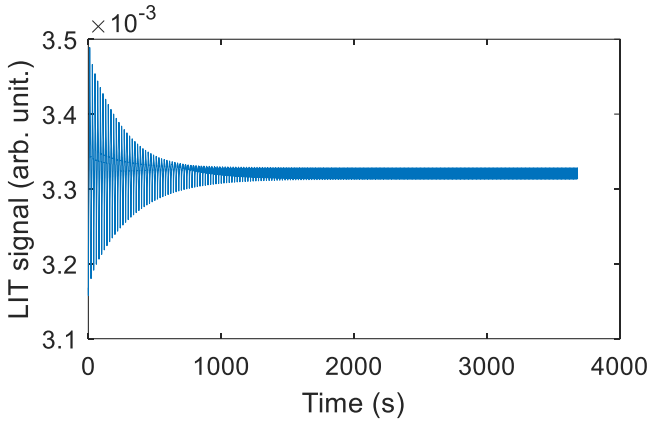

Fig. 9. Simulated variation of a lock-in signal from the beginning of the laser illumination to 3680 s. Each point is calculated over 16 periods at 0.05 Hz laser frequency modulation for a fused silica sample with 1 ppm of absorption. The uncertainty is calculated considering the minimum and the maximum envelope of the signal.

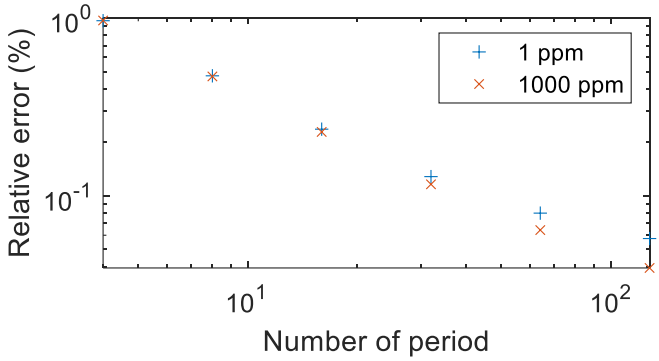

Fig. 10. Simulated variation of a lock-in signal error calculated for different numbers of lock-in periods at 0.05 Hz laser frequency modulation for a fused silica with 1 ppm and 1000 ppm of absorption.

Concerning the uncertainty of the laser power, we need to consider the power fluctuations during the measurement. Typically, this value is ±2% of the mean value. Considering a uniform distribution of power inside the upper and lower limits, this leads to a relative uncertainty on power of $\sigma_{RP} = \frac{Relative\ error}{2\sqrt{3}} = 0.6\ \%$.

We then estimated the uncertainty of the calibration curve parameters (i.e., the uncertainty of a and b in equation 2). Using the values of the uncertainty of the measured signal, incident power, and absorption on the reference sample, we generated a set of randomly shifted values considering a normal distribution for each point of the calibration curve. These points were used to determine several sets of calibration factors. The associated relative standard deviations a and b are 72% and 8%, respectively.

Finally, to obtain the total standard deviation of the absorption, we apply the uncertainty propagation formula [45]:

$$\sigma_A{}^2 = \left(\frac{\partial A}{\partial a}\right)^2 \sigma_a{}^2 + \left(\frac{\partial A}{\partial b}\right)^2 \sigma_b{}^2 + \left(\frac{\partial A}{\partial s}\right)^2 \sigma_s{}^2 + \left(\frac{\partial A}{\partial P}\right)^2 \sigma_P{}^2 + 2\frac{\partial A}{\partial s}\frac{\partial A}{\partial P}\,\sigma_s\,\sigma_P\,Corr(s,P) \quad (5)$$

$$\sigma_A{}^2 = \left(\frac{S}{P}\right)^2 \left[s^2\sigma_a{}^2 + \sigma_b{}^2 + \left(2a + \frac{b}{s}\right)^2 \sigma_s{}^2 + \left(\frac{as+b}{P}\right)^2 \sigma_P{}^2 + 2\left(\frac{2a^2s^2 + 3abs + b^2}{SP}\right)\sigma_s\,\sigma_P\,Corr(s,P)\right] \quad (6)$$

Where $Corr(s,P)$ is the correlation coefficient between s and P. We replace the standard deviation σ_x with a relative form, $\sigma_{Rx} = \sigma_x/x$.

$$\sigma_A{}^2 = \left(\frac{S}{P}\right)^2 \left[s^2\sigma_{Ra}{}^2 + b^2\sigma_{Rb}{}^2 + (2as+b)^2\sigma_{Rs}{}^2 + (as+b)^2\sigma_{RP}{}^2 + 2(2a^2s^2 + 3abs + b^2)\,\sigma_{Rs}\,\sigma_{RP}\,Corr(s,P)\right] \quad (7)$$

We can approximate this relation considering the low value of a, approximately 10^{-6}, and a perfect correlation between the signal and power as follows:

$$\sigma_A{}^2 \approx \left(\frac{S}{P}\right)^2 b^2\left(\sigma_{Rb}{}^2 + (\sigma_{Rs} + \sigma_{RP})^2\right) \quad (8)$$

Therefore, the relative uncertainty is

$$\sigma_{RA} \approx \frac{b}{as+b}\sqrt{\left(\sigma_{Rb}{}^2 + (\sigma_{Rs} + \sigma_{RP})^2\right)} \quad (9)$$

Assuming that the term $a{\cdot}s$ is low compared to b, we obtain

$$\sigma_{RA} \approx \sqrt{\sigma_{Rb}{}^2 + (\sigma_{Rs} + \sigma_{RP})^2} \quad (10)$$

Based on the uncertainty measurements of s, P, and b, the relative uncertainty of A is 11.7%. That uncertainty was obtained by using the worst uncertainty estimation for the signal (8 %), power (0.6 %), and calibration($\sigma_{Ra} = 72\ \%$ and $\sigma_{Rb} = 8\ \%$).

4. APPLICATION TO ABSORPTION MEASUREMENT OF SINGLE-LAYER COATINGS

A. Experimental conditions

Single layers were fabricated with a Bühler SYRUSpro 710 deposition machine using plasma-assisted electron beam deposition. The layers were deposited on a fused silica substrate (Corning 7980) at an O_2 partial pressure of 25 standard cubic centimeters per minute (sccm). The starting deposition pressure was below 10^{-5} mbar. All constituents were evaporated from bulk materials with 99.9% purity. Silica was evaporated directly from a copper crucible, and high-refractive-index materials were evaporated using a molybdenum liner. The deposition rate for silica was 0.5 nm/s and that for high-refractive-index materials was 0.25 nm/s. All other parameters were as recommended by the manufacturer.

The LIT measurements were realized with a 0.05 Hz laser frequency and a power of 150 W was applied during 16 periods of modulation while 2048 sample points are taken. As a preliminary measurement, we characterized the absorption of an uncoated fused silica substrate. An absorption value of approximately 2 ppm was obtained. This value contributed to the total measured absorption.

We completed the LIT measurements with a cavity ring down (CRD) measurement at 1064 nm. CRD is a way to determine a low optical loss level by measuring the decay with time of the laser pulse intensity into an optical cavity [17,46–50]. We used a commercial CRD (LossPro, Novawave Technologies, USA). The uncertainty we associate with this instrument comes from repeatability tests and is about 25 ppm. We calculated the scattering by subtracting the absorption, measured with LIT, from the losses.

B. Absorption of Nb_2O_5 single layers deposited by plasma-assisted electron beam deposition

We first investigated the fluctuation of absorption between the samples coated simultaneously. Fused silica substrates were coated together with a 300 nm single layer of Nb_2O_5 and placed along the same radius of the substrate holder in order to achieve the most uniform deposition conditions. LIT and CRD measurements were performed on the 11 fabricated samples, and the results are presented in Table 1. Comparable absorption values ranging from 13 to 24 ppm are demonstrated, showing that there is a mild absorption variation from sample to sample. These fluctuations in absorption can most likely be explained by particle contamination. The scattering remained stable within the 100–200 ppm range.

Second, we investigated how absorption fluctuated from one coating run to another. Six consecutive coating runs were carried out with nominally the same process parameters and conditions, paying specific attention to the cleanliness of the process. LIT and CRD measurements were performed on each sample, and the measured absorptions are presented in Table 2. Larger fluctuations were observed (approximately three-fold) compared to samples fabricated within the same coating run, but these values remain within the same order of magnitude. These fluctuations can be easily explained by the imperfect repeatability of the experimental conditions, such as the amount of raw material in the crucible, slightly different material state after crucible premelting, preparation, and cleanliness of the Advanced Plasma Source (APS) anode tube. Scattering shows up to twice the value compared to run 1, which can be explained by particles contamination.

Table 1 : Absorption and scattering measured by LIT and CRD of 300 nm Nb_2O_5 single layer samples deposited in a same run.

	Absorption (ppm)	Scattering (ppm)
S1	25 ± 3	155 ± 25
S2	34 ± 4	144 ± 25
S3	22 ± 2	155 ± 25
S4	20 ± 2	112 ± 25
S5	17 ± 2	205 ± 25
S6	21 ± 2	58 ± 25
S7	24 ± 3	243 ± 25
S8	13 ± 1	146 ± 25
S9	19 ± 2	162 ± 25
S10	21 ± 2	245 ± 25
S11	23 ± 3	127 ± 25

Table 2. Absorption and scattering measured by LIT and CRD of 300 nm Nb_2O_5 single layer samples deposited in different runs. The result of Run 1 is the average value of the results shown in Table 1.

	Absorption (ppm)	Scattering (ppm)
Run 1	21 ± 2	159 ± 25
Run 2	28 ± 3	320 ± 25
Run 3	17 ± 2	192 ± 25
Run 4	42 ± 5	596 ± 25
Run 5	34 ± 4	324 ± 25
Run 6	49 ± 5	113 ± 25

C. LIT measurements on single layers of various materials deposited by plasma assisted electron beam deposition

Single layers made of different materials that are classically used for the production of laser coatings, HfO_2, Ta_2O_5, TiO_2, Nb_2O_5, and SiO_2, were investigated. Two sets of samples with thicknesses of 300 and 600 nm were produced. Their absorption was measured using the LIT setup, and the results are reported in Table 3.

Table 3. Absorption and refractive index at 1070 nm measured on HfO_2, Ta_2O_5, TiO_2, Nb_2O_5 and SiO_2 single layers made with plasma-assisted electron beam deposition and with different thicknesses (300 and 600 nm).

Materials	Absorption (ppm)		Refractive index
	300 nm	**600 nm**	
HfO_2	18 ± 2	29 ± 3	1.89
Ta_2O_5	2.4 ± 0.3	18 ± 2	2.12
TiO_2	27 ± 3	33 ± 4	2.25
Nb_2O_5	21 ± 2	21 ± 2	2.20
SiO_2	5.1 ± 0.6	7.6 ± 0.8	1.48

First, one can notice the maximum absorption measured in all samples does not exceed ~30 ppm. All samples with 600 nm thickness have close or larger absorption than those made with the same material, but with 300 nm thickness, confirming that the larger the thickness, the larger the absorption. However, one might expect that increasing the thickness would increase the absorption by a factor of approximately two by considering that the laser intensity into the layer is constant. This assumption is not respected. The increase is about 60 % for HfO_2 and 50 % for SiO_2. The increase can be negligible for Nb_2O_5 or ten-fold as for Ta_2O_5. These differences, which have already been noted and discussed in the previous section, are probably related to some fluctuation of the sample cleanliness or process repeatability and due to the interference effects that also contribute to a modulation of the total absorbed power with thickness [51]. However, the following preliminary conclusions may be drawn:

- As expected, SiO_2 has very low absorption in near-IR and is therefore an interesting low-refractive-index material for CW laser applications.
- Ta_2O_5 appears to be a high-refractive-index material with the lowest absorption. While these results cannot be generalized, they tend to show that with our deposition process, thin-film filters may be produced with minimized laser-induced effects.
- TiO_2, the material with the highest refractive index at the considered wavelength (2.25 at 1.07 µm) [52], shows the largest absorption among the measured samples.
- Others materials (HfO_2-Nb_2O_5) have the same absorption level, within 10%.

These values are in line with those reported for HfO_2 [18,41,53], Ta_2O_5 [18,54,55] TiO_2 [17,52,53], and SiO_2 [18,56,57]. Values under the ppm level were reported for Virgo optics as an example, but on multilayer mirrors with very specific substrate and deposition parameters [58].

D. Comparison of LIT measurement on SiO_2 layers made with plasma-assisted reactive magnetron sputtering and plasma-assisted electron beam deposition

Two sets of SiO_2 single layers with thicknesses ranging from 200 to 1000 nm were fabricated. One was deposited using plasma-assisted reactive magnetron sputtering (Bühler HELIOS) and the other using plasma-assisted electron beam deposition (Bühler SYRUSpro). The thickness was monitored using an optical monitoring system on a pre-coated sample with a Nb_2O_5 single layer. The measurements were performed with the same LIT configuration as that described in the previous section. Fig. 11 shows the results of the LIT images. The ability of the LIT setup to map the local absorption of the samples allows the identification of many hotspots on sputtered SiO_2 samples corresponding to local defects. The absorption of these local defects could not be precisely determined because we do not have information on the nature of these defects (emissivity, size), but it was several times higher than the intrinsic absorption of the layer. In Fig. 11, the sputtered samples show defects in each image. For comparison, only the 1000 nm thickness evaporated sample presented one absorbing defect within the measurement window. Owing to the deposition geometry, plasma-assisted reactive magnetron sputtering technology is known to produce defects that degrade coating cosmetics [59]. We show here that these defects also have a strong influence on the local absorption of the fabricated samples. The overall heating, as shown in the LIT image, is twice higher for samples prepared by plasma-assisted electron beam deposition than for magnetron sputtering. However, several hotspots were visible on the samples prepared by magnetron sputtering, which generated additional heating.

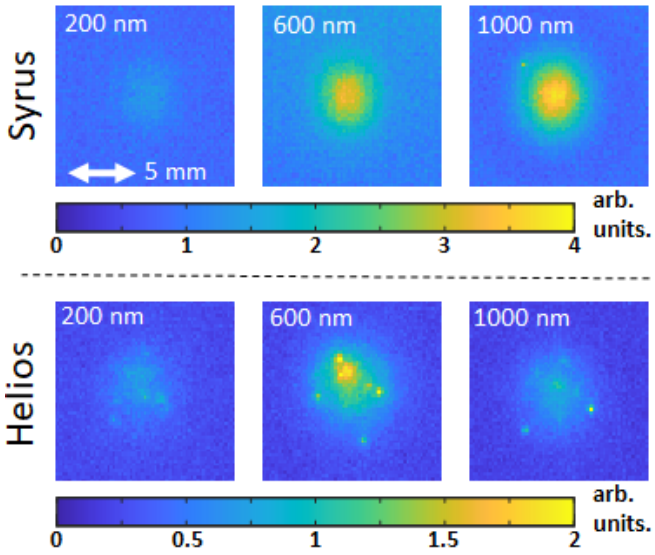

Fig. 11. LIT images for SiO_2 single layers made by plasma-assisted reactive magnetron sputtering (HELIOS) and plasma-assisted electron beam deposition (SYRUS). The HELIOS deposition shows more local defects than SYRUS one.

E. Effect of annealing on the absorption of amorphous layers

The annealing of optical coatings is a classical way to modify the density [60], stoichiometry [61] and losses [62–65] of amorphous thin films. Therefore, we studied the effect of annealing conditions on the absorption of high-index materials. We used a standard regulated resistance furnace (Gravimetric Furnace LG, LAC) to anneal 300 nm thick single layers of Nb_2O_5 and Ta_2O_5 on a same run. The annealing treatments were conducted at atmospheric pressure and ambient atmosphere. Nb_2O_5 has a crystallization temperature around 400°C and Ta_2O_5 around 600°C [63–66]. Hence, different temperatures below 400°C were tested, to remain below the crystallization limit of Nb_2O_5.
The experiment was designed to study the effect of the annealing time. The samples were heated to 400°C at a rate of 10°C/min and then maintained at 400°C for 1, 3, and 6 h before switching off the heating and allowing the furnace to cool to room temperature. The absorption was measured using the LIT setup before and after annealing, and the measured values are listed in

Table 4. A clear effect of the reduction of absorption can be observed for Ta_2O_5, but this effect is very weak for Nb_2O_5, and no effect of annealing time is shown.

By analyzing the transmission spectrum obtained with a Perkin Elmer Lambda 1050 spectrophotometer, we could deduce the variation in the refractive index and the thickness of the layers [67]. The refractive index increased by approximately 10^{-2} while the thickness decreased by a few percent of the initial thickness. This is consistent with the literature, where annealing can densify the layers and lead to an increase in the refractive index [60].

Table 4 : Variations in absorption due to different annealing time (at 400°C) for 300 nm single layers of Ta_2O_5 and Nb_2O_5.

Materials	Annealing Time	Absorption measurements (ppm)		Refractive index variation	Thick. variation (%)
		As deposited	Annealed		
Ta_2O_5	1 h	26	9	$+7.9\times10^{-3}$	–0.93
	3 h	25	13	$+6.6\times10^{-3}$	–0.87
	6 h	25	10	$+6.5\times10^{-3}$	–0.87
Nb_2O_5	1 h	22	19	$+1.9\times10^{-2}$	–1.4
	3 h	34	25	$+2.2\times10^{-2}$	–1.6
	6 h	25	22	$+3.0\times10^{-2}$	–1.9

5. CONCLUSION

An LIT system for the measurement of small absorption in optical coatings was demonstrated. This system relies on the use of a high-power CW laser at 1.07 µm and up to 1500 W of output power. Based on a multipass configuration that recycles the laser power, this system allows the measurement of absorption at the ppm level with an 11 % precision. It was used to measure absorption down to 2 ppm, but could go down to 0.1 ppm or below by using the maximum power available on our laser. The system was also used to map the absorption of the coated samples and reveal potential local defects.

A dedicated calibration method was developed based on the measurement of the LIT signal on a reference sample for different absorbed powers. These calibrated samples were developed using our deposition systems to guarantee that they have similar thermal properties. Various single layers made by plasma-assisted electron beam deposition were investigated with the LIT system (SiO_2, Nb_2O_5, HfO_2, Ta_2O_5, and TiO_2). Repeatability between samples within a coating run and several runs was also investigated. We showed that the measured absorption is within the 10 ppm range and does not fluctuate by more than two to three times among samples. SiO_2 and Ta_2O_5 appeared as low- and high-refractive-index materials with the lowest absorption, respectively. Annealing was confirmed to be an efficient method for further decreasing the absorption.

Funding.

This work was carried out within the LabTOP (Laboratoire commun de Traitement OPtique des surfaces), a research cooperation agreement between the Institut Fresnel (Aix-Marseille Univ, CNRS, Centrale Marseille) and CILAS Ariane Group.

Acknowledgments.

The authors acknowledge Olivier Hector and Cihan Koc for assistance in depositing the samples, Cilas for manufacturing certain samples, and Faris Abouakil and Paul Rouquette for their kind help in evaluating the uncertainties.

Disclosures.

The authors declare no conflicts of interest.

References

1. T. H. Maiman, "Stimulated Optical Radiation in Ruby," Nature **187**, 493–494 (1960).
2. J. W. Dawson, M. J. Messerly, R. J. Beach, M. Y. Shverdin, E. A. Stappaerts, A. K. Sridharan, P. H. Pax, J. E. Heebner, C. W. Siders, and C. P. J. Barty, "Analysis of the scalability of diffraction-limited fiber lasers and amplifiers to high average power," Opt. Express **16**, 13240 (2008).
3. M. N. Zervas and C. A. Codemard, "High Power Fiber Lasers: A Review," IEEE Journal of Selected Topics in Quantum Electronics **20**, 219–241 (2014).
4. A. Godard, "Infrared (2–12 µm) solid-state laser sources: a review," Comptes Rendus Physique **8**, 1100–1128 (2007).
5. J. J. Coleman, A. C. Bryce, and C. Jagadish, eds., *Advances in Semiconductor Lasers*, 1st ed, Semiconductors and Semimetals No. v. 86 (Elsevier/Academic Press, 2012).

6. B. Zohuri, "High-Power Laser Energy," in *Thermal Effects of High Power Laser Energy on Materials* (Springer International Publishing, 2021), pp. 1–25.
7. C. N. Danson, C. Haefner, J. Bromage, T. Butcher, J.-C. F. Chanteloup, E. A. Chowdhury, A. Galvanauskas, L. A. Gizzi, J. Hein, D. I. Hillier, N. W. Hopps, Y. Kato, E. A. Khazanov, R. Kodama, G. Korn, R. Li, Y. Li, J. Limpert, J. Ma, C. H. Nam, D. Neely, D. Papadopoulos, R. R. Penman, L. Qian, J. J. Rocca, A. A. Shaykin, C. W. Siders, C. Spindloe, S. Szatmári, R. M. G. M. Trines, J. Zhu, P. Zhu, and J. D. Zuegel, "Petawatt and exawatt class lasers worldwide," High Power Laser Science and Engineering **7**, e54-undefined (2019).
8. N. Fleurot, C. Cavailler, and J. L. Bourgade, "The Laser Mégajoule (LMJ) Project dedicated to inertial confinement fusion: Development and construction status," Fusion Engineering and Design **74**, 147–154 (2005).
9. C. A. Haynam, P. J. Wegner, J. M. Auerbach, M. W. Bowers, S. N. Dixit, G. V. Erbert, G. M. Heestand, M. A. Henesian, M. R. Hermann, K. S. Jancaitis, K. R. Manes, C. D. Marshall, N. C. Mehta, J. Menapace, E. Moses, J. R. Murray, M. C. Nostrand, C. D. Orth, R. Patterson, R. A. Sacks, M. J. Shaw, M. Spaeth, S. B. Sutton, W. H. Williams, C. C. Widmayer, R. K. White, S. T. Yang, and B. M. Van Wonterghem, "National Ignition Facility laser performance status," Appl. Opt. **46**, 3276 (2007).
10. A. Feicker, *U.S. Army Weapons-Related Directed Energy(DE) Programs: Background and Potential Issues for Congress* (Congressional Research Service, 2018).
11. L. Lazov and E. Teirumnieks, "Application of laser technology in the army," in *Proceedings of International Scientific Conference "Defense Technologies"* (2018).
12. G. Jimenez, "Determining the feasability of an army laser air and missile defence system," West Point (2019).
13. E. A. Shcherbakov, V. V. Fomin, A. A. Abramov, A. A. Ferin, D. V. Mochalov, and V. P. Gapontsev, "Industrial grade 100 kW power CW fiber laser," in *Advanced Solid-State Lasers Congress* (OSA, 2013), p. ATh4A.2.
14. D. Ristau, M. Jupé, and K. Starke, "Laser damage thresholds of optical coatings," Thin Solid Films **518**, 1607–1613 (2009).
15. O. Stenzel and M. Ohlídal, eds., *Optical Characterization of Thin Solid Films*, Springer Series in Surface Sciences (Springer International Publishing, 2018), Vol. 64.
16. L. A. Skvortsov, "Laser photothermal spectroscopy of light-induced absorption," Quantum Electron. **43**, 1–13 (2013).
17. H. Cui, B. Li, S. Xiao, Y. Han, J. Wang, C. Gao, and Y. Wang, "Simultaneous mapping of reflectance, transmittance and optical loss of highly reflective and anti-reflective coatings with two-channel cavity ring-down technique," Opt. Express **25**, 5807 (2017).
18. D. Ristau and J. Ebert, "Development of a thermographic laser calorimeter," Appl. Opt. **25**, 4571 (1986).
19. "Lasers and laser-related equipment, test method for absorptance of optical laser components," ISO **ISO11551**, (2019).
20. N. K. Sahoo and K. V. S. R. Apparao, "Laser calorimeter for UV absorption measurement of dielectric thin films," Appl. Opt. **31**, 6111 (1992).
21. M. Commandré and E. Pelletier, "Measurements of absorption losses in TiO_2 films by a collinear photothermal deflection technique," Appl. Opt. **29**, 4276 (1990).
22. S. Bublitz and C. Mühlig, "Absolute Absorption Measurements in Optical Coatings by Laser Induced Deflection," Coatings **9**, 473 (2019).
23. Z. L. Wu, M. Reichling, X.-Q. Hu, K. Balasubramanian, and K. H. Guenther, "Absorption and thermal conductivity of oxide thin films measured by photothermal displacement and reflectance methods," Appl. Opt. **32**, 5660 (1993).
24. W. B. Jackson, N. M. Amer, A. C. Boccara, and D. Fournier, "Photothermal deflection spectroscopy and detection," Appl. Opt. **20**, 1333 (1981).
25. J. Dong, R. Lu, T. Zhang, L. Yang, Y. Zhang, Z. Wu, and J. Chen, "Multi-channel averaging detection for fast imaging of weakly absorbing defects in surface thermal lensing," Review of Scientific Instruments **89**, 114904 (2018).
26. F. Z. Escola, N. Míngolo, O. E. Martínez, J. J. Rocca, and C. S. Menoni, "Characterization of absorptance homogeneity in thin-film coatings for high-power lasers by thermal lensing microscopy," Appl. Opt. **58**, 7233 (2019).
27. M. Leidinger, S. Fieberg, N. Waasem, F. Kühnemann, K. Buse, and I. Breunig, "Comparative study on three highly sensitive absorption measurement techniques characterizing lithium niobate over its entire transparent spectral range," Opt. Express **23**, 21690 (2015).
28. N. Lastzka, J. Steinlechner, S. Steinlechner, and R. Schnabel, "Measuring small absorptions by exploiting photothermal self-phase modulation," Appl. Opt. **49**, 5391 (2010).
29. J. Steinlechner, L. Jensen, C. Krüger, N. Lastzka, S. Steinlechner, and R. Schnabel, "Photothermal self-phase-modulation technique for absorption measurements on high-reflective coatings," Appl. Opt. **51**, 1156 (2012).
30. N. Waasem, S. Fieberg, J. Hauser, G. Gomes, D. Haertle, F. Kühnemann, and K. Buse, "Photoacoustic absorption spectrometer for highly transparent dielectrics with parts-per-million sensitivity," Review of Scientific Instruments **84**, 023109 (2013).
31. A. V. Konyashkin, A. A. Molkov, and O. A. Ryabushkin, "Acoustic resonance laser calorimetry for measurements of low optical absorption," Appl. Opt. **59**, 8733 (2020).
32. S. Fieberg, N. Waasem, F. Kühnemann, and K. Buse, "Sensitive absorption measurements in bulk material and coatings using a photothermal and a photoacoustic spectrometer," in K. L. Vodopyanov, ed. (2014), p. 896410.
33. A. F. Stewart and W. Hughes, "Measurement of low-absorption optics by thermal imaging," in G. J. Exarhos, A. H. Guenther, K. L. Lewis, D. Ristau, M. J. Soileau, and C. J. Stolz, eds. (2006), p. 64031H.
34. R. Fuente, A. Mendioroz, E. Apiñaniz, and A. Salazar, "Simultaneous Measurement of Thermal Diffusivity and Optical Absorption Coefficient of Solids Using PTR and PPE: A Comparison," Int J Thermophys **33**, 1876–1886 (2012).
35. O. Breitenstein, W. Warta, and M. Langenkamp, *Lock-in Thermography*, Springer Series in Advanced Microelectronics (Springer Berlin Heidelberg, 2010), Vol. 10.
36. F. Liu and L. Gallais, "Absorption measurements in optical coatings by lock-in thermography," Appl. Opt. **56**, 9225 (2017).
37. M. Lax, "Temperature rise induced by a laser beam," Journal of Applied Physics **48**, 3919–3924 (1977).
38. C. Wei, "Study of thermal behaviors in CO2 laser irradiated glass," Opt. Eng **44**, 044202 (2005).
39. M. D. Feit and A. M. Rubenchik, "Mechanisms of CO 2 laser mitigation of laser damage growth in fused silica," in G. J. Exarhos, A. H. Guenther, N. Kaiser, K. L. Lewis, M. J. Soileau, C. J. Stolz, A. Giesen, and H. Weber, eds. (2003), p. 91.
40. *Corning® HPFS® 7979, 7980, 8655 Fused Silica - Optical Materials Product Information* (Corning - Specialty Materials, 2015).
41. S. Papernov, M. D. Brunsman, J. B. Oliver, B. N. Hoffman, A. A. Kozlov, S. G. Demos, A. Shvydky, F. H. M. Cavalcante, L. Yang, C. S. Menoni, B. Roshanzadeh, S. T. P. Boyd, L. A. Emmert, and W. Rudolph, "Optical properties of oxygen vacancies in HfO2 thin films studied by absorption and luminescence spectroscopy," Opt. Express **26**, 17608 (2018).
42. F. Z. Escola, N. Mingolo, O. E. Martínez, J. J. Rocca, and C. S. Menoni, "Investigation of laser annealing mechanisms in thin film coatings by photothermal microscopy," Opt. Express **27**, 5729 (2019).
43. L. Gallais and M. Commandré, "Simultaneous absorption, scattering, and luminescence mappings for the characterization of optical coatings and surfaces," Appl. Opt. **45**, 1416 (2006).
44. *Evaluation of Measurement Data — Supplement 1 to the "Guide to the Expression of Uncertainty in Measurement" — Propagation of Distributions Using a Monte Carlo Method*, BIPM, JCGM 101:2008 (2008).

45. "Evaluation of measurement data — Guide to the expression of uncertainty in measurement," BIPM **JCGM 100:2008**, 20 (2008).
46. J. M. Herbelin, J. A. McKay, M. A. Kwok, R. H. Ueunten, D. S. Urevig, D. J. Spencer, and D. J. Benard, "Sensitive measurement of photon lifetime and true reflectances in an optical cavity by a phase-shift method," Appl. Opt. **19**, 144 (1980).
47. D. Z. Anderson, J. C. Frisch, and C. S. Masser, "Mirror reflectometer based on optical cavity decay time," Appl. Opt. **23**, 1238 (1984).
48. G. A. Marcus and H. A. Schwettman, "Cavity ringdown spectroscopy of thin films in the mid-infrared," Appl. Opt. **41**, 5167 (2002).
49. G. Berden and R. Engeln, eds., *Cavity Ring-down Spectroscopy: Techniques and Applications* (Wiley, 2009).
50. A. O'Keefe and D. A. G. Deacon, "Cavity ring-down optical spectrometer for absorption measurements using pulsed laser sources," Review of Scientific Instruments **59**, 2544–2551 (1988).
51. F. Geng, H. Cheng, Q. Zhang, M. Liu, and A. Y. Li, "Ultraviolet laser damage properties of single-layer SiO2 film grown by atomic layer deposition," Opt. Mater. Express **10**, 1981 (2020).
52. T. Siefke, S. Kroker, K. Pfeiffer, O. Puffky, K. Dietrich, D. Franta, I. Ohlídal, A. Szeghalmi, E. Kley, and A. Tünnermann, "Materials Pushing the Application Limits of Wire Grid Polarizers further into the Deep Ultraviolet Spectral Range," Advanced Optical Materials **4**, 1780–1786 (2016).
53. Q. Zhang, F. Pan, J. Luo, Q. Wu, Z. Wang, and Y. Wei, "Optical and laser damage properties of HfO2/Al2O3 thin films deposited by atomic layer deposition," Journal of Alloys and Compounds **659**, 288–294 (2016).
54. V. V. Novopashin, L. A. Skvortsov, and M. I. Skvortsova, "Effect of composition nonstoichiometry on the optical properties of titanium dioxide films," J. Opt. Technol. **85**, 803 (2018).
55. B. Cimma, D. Forest, P. Ganau, B. Lagrange, J.-M. Mackowski, C. Michel, J.-L. Montorio, N. Morgado, R. Pignard, L. Pinard, and A. Remillieux, "Ion beam sputtering coatings on large substrates: toward an improvement of the mechanical and optical performances," Appl. Opt. **45**, 1436 (2006).
56. F. Z. Escola, N. Mingolo, O. E. Martínez, J. J. Rocca, and C. S. Menoni, "Absorptance homogeneity and its relaxation in thin films by photothermal microscopy," in *Optical Interference Coatings Conference (OIC) 2019* (OSA, 2019), p. TE.2.
57. K. Pfeiffer, S. Shestaeva, A. Bingel, P. Munzert, L. Ghazaryan, C. van Helvoirt, W. M. M. Kessels, U. T. Sanli, C. Grévent, G. Schütz, M. Putkonen, I. Buchanan, L. Jensen, D. Ristau, A. Tünnermann, and A. Szeghalmi, "Comparative study of ALD SiO_2 thin films for optical applications," Opt. Mater. Express **6**, 660 (2016).
58. L. Pinard, C. Michel, B. Sassolas, L. Balzarini, J. Degallaix, V. Dolique, R. Flaminio, D. Forest, M. Granata, B. Lagrange, N. Straniero, J. Teillon, and G. Cagnoli, "Mirrors used in the LIGO interferometers for first detection of gravitational waves," Appl. Opt. **56**, C11 (2017).
59. H. Krol, C. Grèzes-Besset, D. Torricini, and D. Stojcevski, "High performances optical coatings with dual ion beam sputtering technique," in M. Lequime, H. A. Macleod, and D. Ristau, eds. (2015), p. 96270L.
60. S. B. Khan, Z. Zhang, and S. L. Lee, "Annealing influence on optical performance of HfO2 thin films," Journal of Alloys and Compounds **816**, 152552 (2020).
61. A. Paolone, E. Placidi, E. Stellino, M. G. Betti, E. Majorana, C. Mariani, A. Nucara, O. Palumbo, P. Postorino, I. Rago, F. Trequattrini, M. Granata, J. Teillon, D. Hofman, C. Michel, A. Lemaitre, N. Shcheblanov, G. Cagnoli, and F. Ricci, "Effects of the annealing of amorphous Ta2O5 coatings produced by ion beam sputtering concerning the effusion of argon and the chemical composition," Journal of Non-Crystalline Solids **557**, 120651 (2021).
62. P. Roche, M. Commandré, L. Escoubas, J. P. Borgogno, G. Albrand, and B. Lazaridès, "Substrate effects on absorption of coated surfaces," Appl. Opt. **35**, 5059 (1996).
63. A. A. Atta, M. M. El-Nahass, A. M. Hassanien, K. M. Elsabawy, M. M. Abd El-Raheem, A. Alhuthali, S. E. Alomariy, and M. S. Algamdi, "Effect of thermal annealing on structural, optical and electrical properties of transparent Nb2O5 thin films," Materials Today Communications **13**, 112–118 (2017).
64. T. Sertel, N. A. Sonmez, S. S. Cetin, and S. Ozcelik, "Influences of annealing temperature on anti-reflective performance of amorphous Ta2O5 thin films," Ceramics International **45**, 11–18 (2019).
65. Y. Pu, P. Ma, Z. Qiao, M. Zhang, Z. Lu, F. Qiu, and L. Lv, "Annealing effects on microstructure and laser-induced damage threshold of quasi-rugate filters," Opt. Express **24**, 23044 (2016).
66. X. Wang, G. Wu, B. Zhou, and J. Shen, "Thermal Annealing Effect on Optical Properties of Binary TiO2-SiO2 Sol-Gel Coatings," Materials **6**, 76–84 (2012).
67. L. Gao, F. Lemarchand, and M. Lequime, "Comparison of different dispersion models for single layer optical thin film index determination," Thin Solid Films **520**, 501–509 (2011).